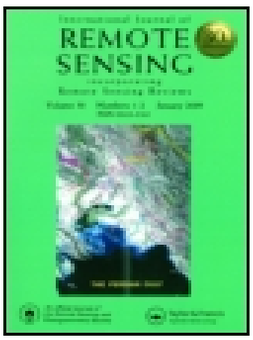

International Journal of Remote Sensing

ISSN: 0143-1161 (Print) 1366-5901 (Online) Journal homepage: http://www.tandfonline.com/loi/tres20

Studies of precipitable water vapour characteristics on a global scale

Qingzhi Zhao, Yibin Yao & Wanqiang Yao

To cite this article: Qingzhi Zhao, Yibin Yao & Wanqiang Yao (2018): Studies of precipitable water vapour characteristics on a global scale, International Journal of Remote Sensing, DOI: 10.1080/01431161.2018.1492177

To link to this article: https://doi.org/10.1080/01431161.2018.1492177

Published online: 02 Aug 2018.

INTERNATIONAL JOURNAL OF REMOTE SENSING
https://doi.org/10.1080/01431161.2018.1492177

Taylor & Francis
Taylor & Francis Group

Studies of precipitable water vapour characteristics on a global scale

Qingzhi Zhao[a], Yibin Yao[b,c] and Wanqiang Yao[a]

[a]College of Geomatics, Xi'an University of Science and Technology, Xi'an, China; [b]School of Geodesy and Geomatics, Wuhan University, Wuhan, China; [c]Key Laboratory of Geospace Environment and Geodesy, Ministry of Education, Wuhan University, Wuhan, China

ABSTRACT

Atmospheric water vapour plays an important role in hydrological, global climate change, atmospheric, and meteorological processes. In this study, precipitable water vapour (PWV) data set for 2004–2017 was first estimated with an average accuracy of about 1.28 mm globally using the products provided by the International Global Navigation Satellite System Service and Global Geodetic Observation System Atmosphere and then the spatio-temporal trends of PWV variation were characterized. Periodic signals of the annual, semi-annual, and seasonal variations of PWV time series were detected based on the Lomb–Scargle periodogram and analysed by dividing the whole world into five geographical zones. From a global perspective, the average PWV has an increasing trend, which may be caused by global warming effects and anthropogenic activities. Analysis of different PWV amplitudes also shows that the main component of the PWV is annual amplitude except in low latitude zones. In addition, the PWV differences between weekends and weekdays for four seasons are also analysed globally, and the result indicates that the weekend effects caused by anthropogenic activity depend on season and region

ARTICLE HISTORY
Received 22 November 2017
Accepted 15 June 2018

1. Introduction

Precipitable water vapour (PWV), which plays an important role in meteorology, climatology, and other meteorological disciplines, is the most abundant greenhouse gas (Ortiz et al., 2011). In addition, the greenhouse effects of water vapour may enhance the response of climate, leading to further global warming (Raval and Ramanathan, 1989; Held and Soden, 2000). Therefore, precise knowledge of PWV characteristics with high spatio-temporal resolution is a prerequisite to better understanding of the importance of water vapour in meteorological fields; however, due to the limited spatio-temporal resolution as well as its being influenced by global warming and anthropogenic activities, the accurate and timeous water vapour distribution data acquisition remains a challenge (Liu et al., 2013; Wong et al., 2015).

Traditional methods for water vapour measurement, including radiosonde, microwave radiometer, etc., are restricted by their low temporal resolution and high cost, so

CONTACT Qingzhi Zhao zhaoqingzhia@163.com Xi'an University of Science and Technology, Xi'an, China

they cannot be used to track temporal variations in water vapour content (Van Baelen et al., 2005), even though those methods can provide high accuracy or vertical resolution (Held and Soden, 2000; Brettle and Galvin, 2003). Therefore, a new technique is exploited, which can be used to obtain additional PWV data using Global Navigation Satellite System (GNSS) observations (Bevis et al., 1992). GNSS-derived PWV data with high spatio-temporal resolution in all weather conditions can be used for the systematic study of atmospheric water vapour characteristics (Jade et al., 2008; Jin et al., 2007; Jakobson et al., 2009; Palau et al., 2017).

Some studies have been performed in analysing the characteristics of PWV distribution in some specific regions, e.g. Indian subcontinent (Jade, et al., 2005; Joshi et al., 2013), the coastal regions of China (Wong et al., 2015; Wang et al., 2017), northeast India (Barman et al., 2017), Taiwan (Yeh et al., 2016); however, detailed analysis on a global scale remains rare. Here, a near-global PWV data set of 192 sites from 2004 to 2017 are first calculated using the International GNSS Service (IGS)-derived zenith total delay (ZTD) and Global Geodetic Observing System (GGOS)-derived surface pressure and water-vapour-weighted mean temperature. The characteristics of PWV average values, annual, semi-annual and seasonal annual amplitudes are analysed on a global scale. In addition, the weekend effects caused by anthropogenic activities are also discussed by combining the distribution of world population from the website of Natural Earth.

2. Data description and PWV calculation

2.1. *IGS ZTD*

The IGS, formerly the International global positioning system (GPS) Service, is a voluntary collaboration of more than 200 contributing organisations in more than 80 countries. The IGS global tracking network of more than 300 permanent, continuously operating (GPS) stations provides rich GNSS data and products of high quality, free of charge, including IGS precise orbits and clocks, and ionosphere and troposphere products. The ZTD products provided are analysed using GPS-Inferred Positioning System Precise Point Positioning software with the IGS final orbits and clocks with an accuracy of better than 7 mm (Byun and BarSever, 2009; Kouba, 2015).

2.2. *GGOS products*

GGOS Atmosphere is an institution which aims to build an atmosphere model and provides the parameters as gridded or model data. Some gridded data are global, such as atmospheric weighted average temperature, linear horizontal gradient, and troposphere delay parameters, which can be obtained with temporal and spatial resolutions of 6 h and 2.5°, respectively. In addition, some model data, such as the coefficients of the Vienna Mapping Function) model, can also be provided by GGOS (Boehm *et al*., 2006). The aforementioned data are acquired from reanalysed data of European Centre for Medium-Range Weather Forecasts of 40 year Re-analysis (ECMWF ERA-40), which considers many types of information: vertical temperature profile radiometer data, Tiros Operational Vertical Sounder data, and conventional ground-based data (radiosonde data) (Yao *et al*., 2014).

2.3. PWV calculation and evaluation

The ZTD data derived from the IGS can be used to extract the zenith wet delay (ZWD) by removing zenith hydrostatic delay (ZHD) calculated based on the empirical model (Saastamoinen, 1972), where ZHD can be expressed as follows:

$$\mathrm{ZHD} = \frac{0.00228P_s}{1 - 0.00266\cos(2\varphi) - 0.00028H} \tag{1}$$

where P_s refers to the surface pressure, which is obtained from the GGOS (unit: hPa), and φ and H represent the latitude and geodetic height of the station, respectively. In addition, the atmospheric weighted mean temperature can also be obtained from the GGOS. Therefore, the PWV of IGS sties can be obtained based on the following formula (Askne and Nordius, 1987):

$$\mathrm{PWV} = \Pi(\mathrm{ZWD}) \tag{2}$$

where Π is the conversion factor, which can be expressed as follows:

$$\Pi = \frac{10^6}{\rho_v R_v \left[k_3/T_m + k_2'\right]} \tag{3}$$

where ρ_v is the density of liquid water (unit: g m^- (Barman et al. 2017)), R_v is the specific gas constant of water vapour with a value of 461.495 (unit: J kg^{-1} K^- (Alshawaf et al. 2017)). k_2' and k_3 are constants, where $k_2' = 22.1 \pm 2.2$ (unit: K Pa^- (Alshawaf et al. 2017)) and $k_3 = 3.739 \pm 0.0012\ 10^5$ (unit: K (Arguez and Vose 2011) Pa^- (Alshawaf et al. 2017)), respectively (Bevis *et al.*, 1992; 1994). T_m denotes the atmospheric weighted mean temperature (unit: K).

In our study, 192 GPS stations are selected to calculate the PWV values, and the quality of the obtained PWV is assessed by using the counterparts derived from radiosonde data. In this comparison, the data from the Integrated Global Radiosonde Archive (IGRA) Version 2 (IGRA 2) are used, which provides more data sources and more time periods. The following gives the procedure to estimate the IGRA 2-PWV, the ZWD and T_m are first calculated based on the following formulas (Bevis et al., 1992; Wang et al., 2016):

$$\mathrm{ZWD} = 373000 \sum (\rho_{v,i}/T_i^2)\ \Delta z_i \tag{4}$$

$$T_m = \frac{\int \frac{e}{T}\,dz}{\int \frac{e}{T^2}\,dz} \approx \frac{\sum \frac{e_i}{T_i}\Delta z_i}{\sum \frac{e_i}{T_i^2}\Delta z_i} \tag{5}$$

where e is the partial pressure of water vapour, $T$is the atmospheric temperature, and i is the ith pressure level. After that, the IGRA 2-PWV can be calculated based on Equations (2) and (3). In this comparison, 97 radiosonde stations are selected from more than 2000 stations worldwide based on the principle that the distance between a radiosonde station and a GPS station is less than 30 km while the altitude difference is less than 100 m. Therefore, there are 97 collocated stations on a global scale used to evaluate the PWV calculated using the IGS and GGOS products. Figure 1 shows the root mean square (RMS) error distribution of PWV differences derived from the proposed method and radiosonde data. It can be observed that the values of RMS are relative

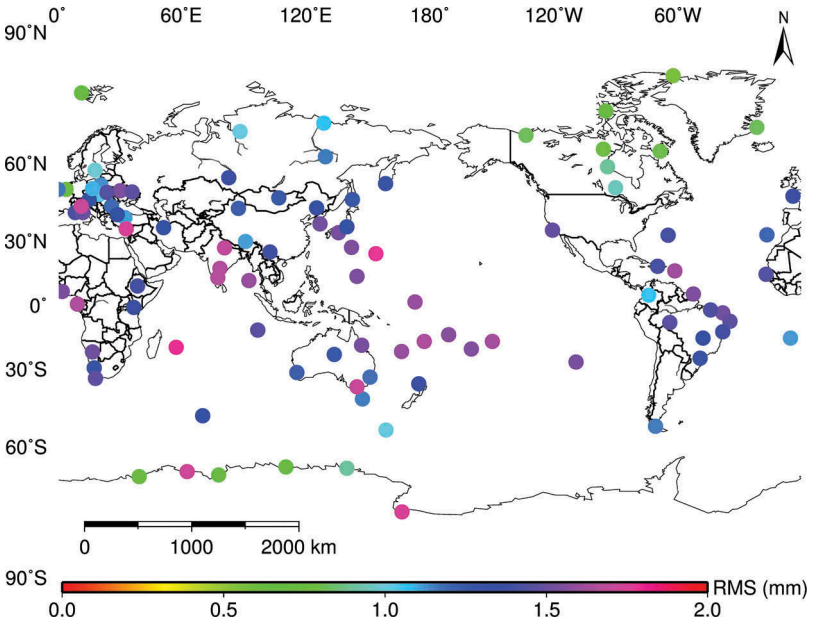

Figure 1. RMS distribution of PWV differences derived from the proposed method and radiosonde data.

large at low latitudes while the values are small at high latitudes. Statistical result shows that the average-maximum-minimum RMS errors are 1.28, 1.83, and 0.58 mm, from 2004 to 2017, respectively. Such accuracy in calculated PWV data is satisfactory.

3. Establishment and evaluation of the PWV model

3.1. *Establishing the PWV model*

As described earlier, PWV exhibits periodic variations and is region-, and altitude-dependent, therefore, the analysis of PWV periodicity on a global scale is required. The Lomb–Scargle periodogram method is used to detect the periodic characteristics of PWV time series, which is similar to Fourier spectrum analysis, but with ability to process the data with uneven sampling intervals or with gaps (Hocke, 1998). Four of the 192 stations are selected randomly on a global scale to present different periodic variations in PWV time series. The names of the selected four stations are TID1, SPT0, NKLG, and PIN1, respectively. Figure 2 shows periodic variations of four stations based on the Lomb–Scargle periodogram method. It can be concluded that stations at different locations are influenced by different periodicity in the PWV time series, which proves that it is acceptable to describe the PWV time series based on a periodic model. In addition, some interesting points can be found in (Figure 2) that (a) TID1 is only determined by the annual periodicity, (b) SPT0 and (c) NKLG include annual and semi-annual periodicities, while (d) PIN1 is influenced by annual, semi-annual and seasonal periodicities. Even for SPT0 and NKLG, which both includes two periodicities, SPT0 is mainly governed by the annual periodicity while NKLG is mainly affected by semi-annual periodicity.

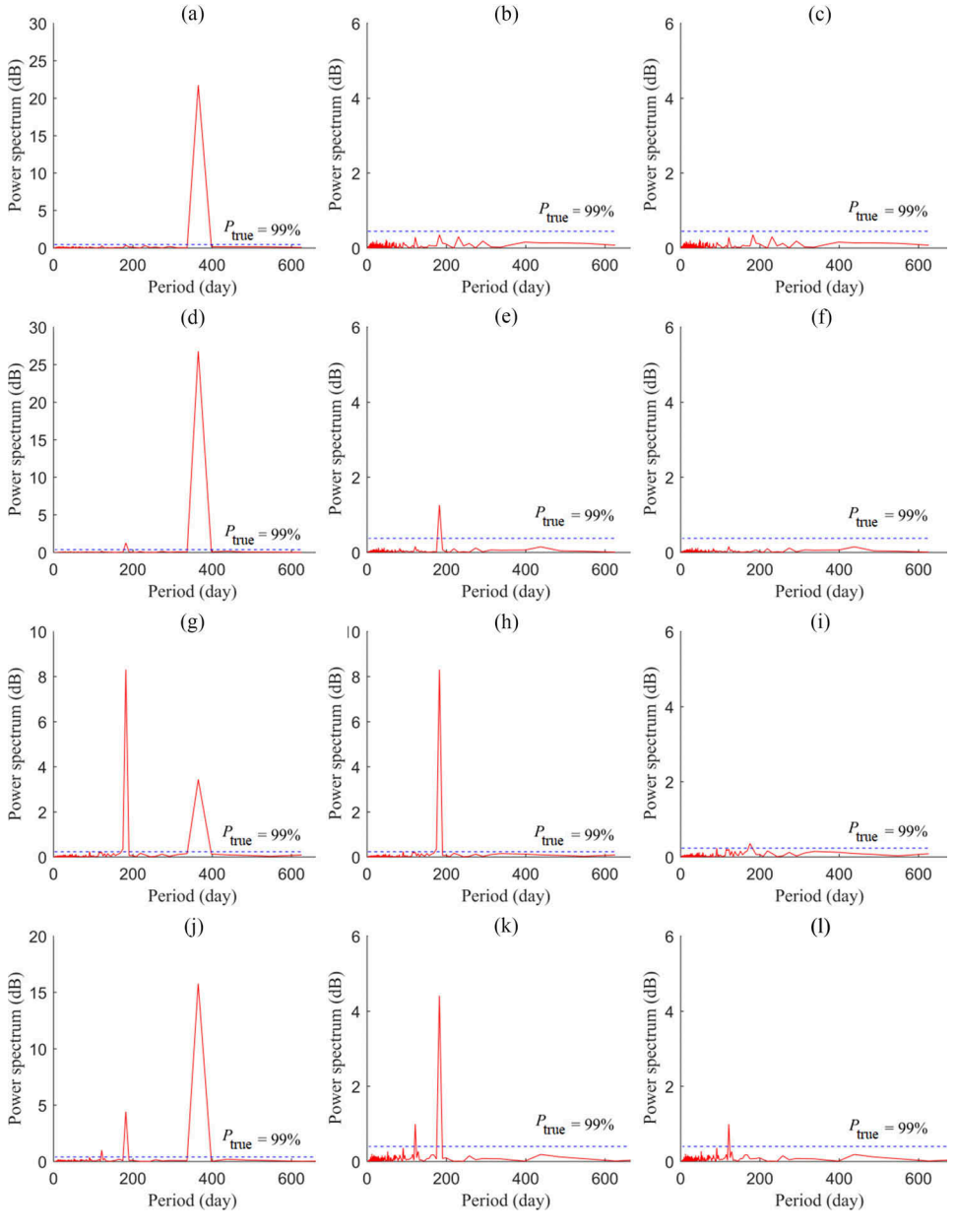

Figure 2. Periodic variations for TID1, SPT0, NKLG, and PINI stations based on the Lomb–Scargle periodogram method, where (a)–(c) correspond to the annual, semi-annual, and seasonal periods of TID1, (d)–(f) correspond to the annual, semi-annual, and seasonal periods of SPT0, (g)–(i) correspond to NKLG, and (j)–(l) correspond to the annual, semi-annual, and seasonal periods of PIN1, respectively.

Therefore, the periodic model of PWV time series for 192 stations can be established, which also considers the trends in the variations of other tropospheric elements, e.g. zenith tropospheric delay (Jin *et al.*, 2007) or atmospheric weighted mean temperature (Ding and Hu, 2017). Finally, the PWV periodic model is determined as a combination of three periodicities and the trend term, which may be expressed as follows:

$$2\mathrm{PWV}(t) = (\mathrm{PWV})0 + v((\mathrm{year}) - (\mathrm{year})_0) + a_1\cos(2\pi(\mathrm{DOY})/365.25 - \varphi_1) + a_2\cos(4\pi(\mathrm{DOY})/365.25 - \varphi_2) + a_3\cos(6\pi(\mathrm{DOY})/365.25 - \varphi_3) \quad (6)$$

where $(\mathrm{PWV})_0$ is the mean value of PWV in the initial year $(\mathrm{year})_0$ (2004 in this study), v is the trend of PWV time series, DOYis the day of year; $a_1 - a_3$ are the annual, semi-annual and seasonal amplitudes, respectively, while $\varphi_1 - \varphi_3$ are the corresponding annual, semi-annual, and seasonal phases, respectively. The unknown parameters in Equation (6) can be estimated by least squares method using the calculated PWV time series mentioned in Section 2.

3.2. *Accuracy analysis of the PWV model*

The established PWV model was first evaluated at each selected site by the index of RMS:

$$\mathrm{RMSE} = \sqrt{\frac{1}{n}\sum_{i=1}^{n}\left((\mathrm{PWV})_{\mathrm{M}}^{\mathrm{i}} - (\mathrm{PWV})_{\mathrm{C}}^{\mathrm{i}}\right)^2} \quad (7)$$

where $(\mathrm{PWV})_{\mathrm{M}}$ refers to the PWV value calculated by the fitted PWV model while $(\mathrm{PWV})_{\mathrm{C}}$ is the calculated PWV value using the IGS and GGOS products, and n is the number of PWV data sets.

It can be seen from Figure 3 that the RMS is related to latitude, where the RMS value is large at the low latitude area while the value is contrary at the high latitude area except at four IGS sites (NKLG, MBAR, NTUS, and BOGT) near the equator, as shown by the red rectangle in Figure 4 (a). In addition, the RMS values are not related to altitude when below 0.5 km but show a negative relationship with altitude above 0.5 km with a

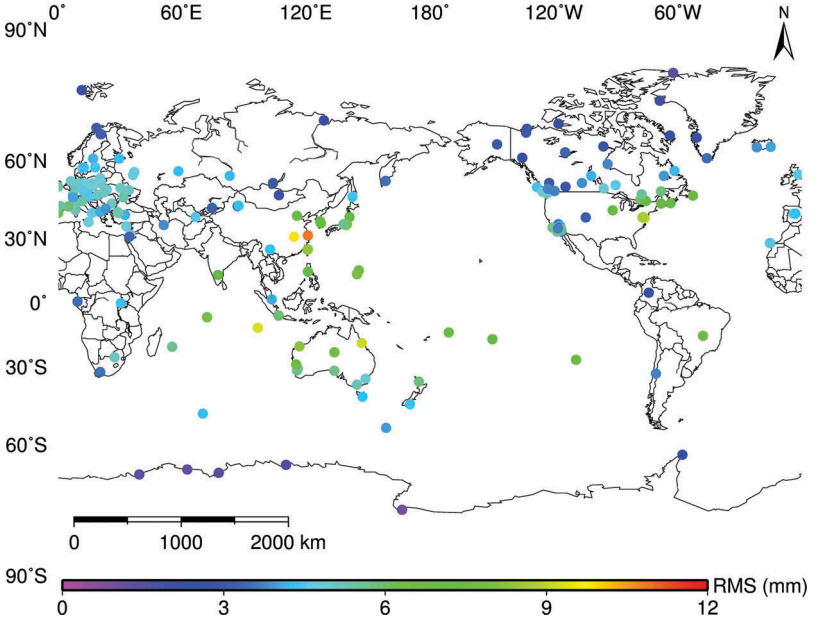

Figure 3. Geographical distribution of RMS.

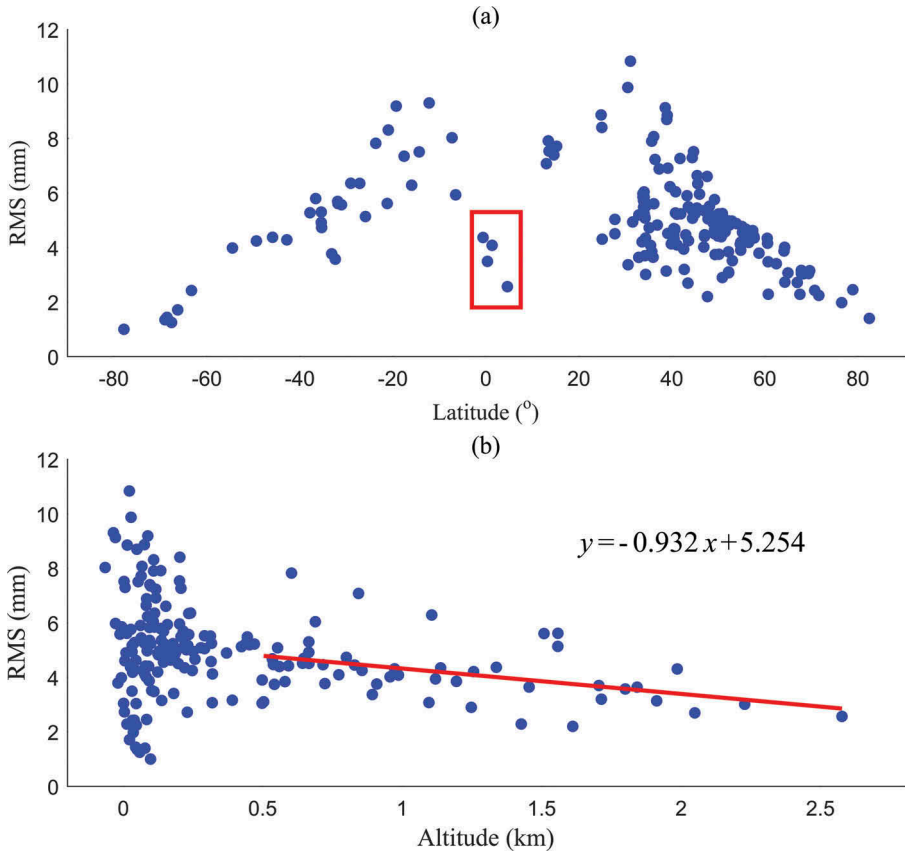

Figure 4. Relationship between (a) RMS and latitude, (b) RMS and altitude.

slope of −0.932 mm km^{-} (Alshawaf et al. 2017). As shown in Figure 4 (a), four sites near the equator showed a relative small RMS, which was mainly caused by the semi-annual amplitude of PWV variation as discussed later.

4. Periodic analysis of PWV

4.1. *Global characteristics of PWV data*

To analyse the characteristics of PWV time series on a global scale, we first divided the global scale into five different geographical zones according to the latitude [Ding and Hu, 2017], which are the North Frigid Zone, the North Temperate Zone, the Tropical Zone, the South Temperate Zone, and the Frigid Zone, respectively. The distribution of PWV mean values is presented while the different zones are divided by red lines in (Figure 5), from which it can be seen that the PWV mean value is highly correlated with latitude. Statistical result shows that PWV mean values for five zones are 7.1, 14.9, 39.6, 14.4, and 3.2 mm, respectively. In addition, Figure 6 also shows the distribution of PWV mean values with latitude and altitude, from which it can be concluded that the average PWV reaches its largest value near the equator and decreases with increasing latitude, but no trend is

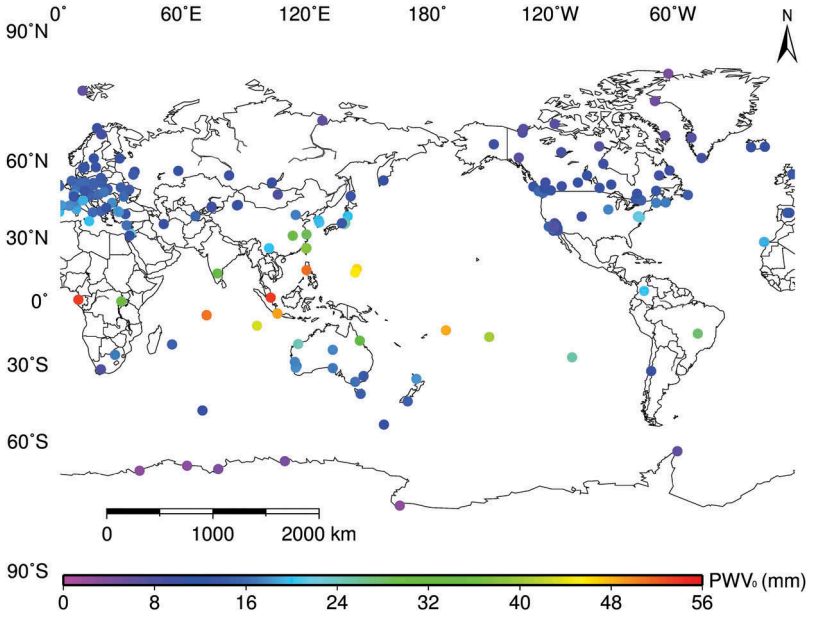

Figure 5. Geographical distribution of PWV mean value on a global scale.

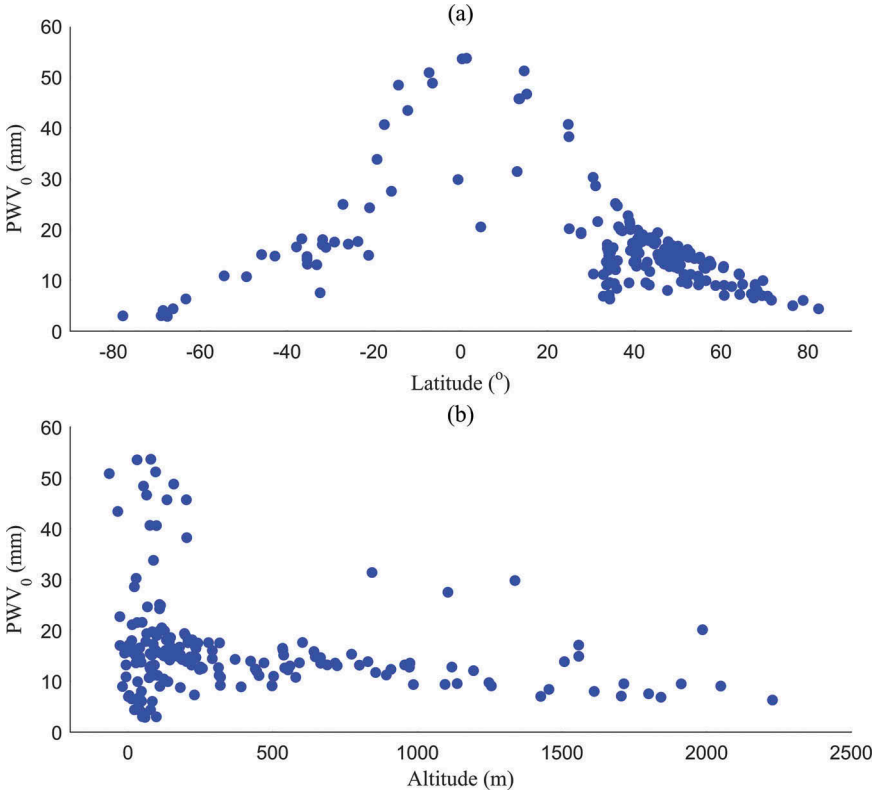

Figure 6. Distribution of PWV mean values with (a) latitude and (b) altitude.

evident with height. In addition, it also can be seen from Figure 6 (b) that the sites with average PWV values greater than 30 mm are distributed between heights of 0 and 300 m.

The annual, semi-annual, and seasonal oscillations of PWV are analysed using coefficients $a_1 - a_3$, respectively. Figures 7–9 show the geographic distribution of

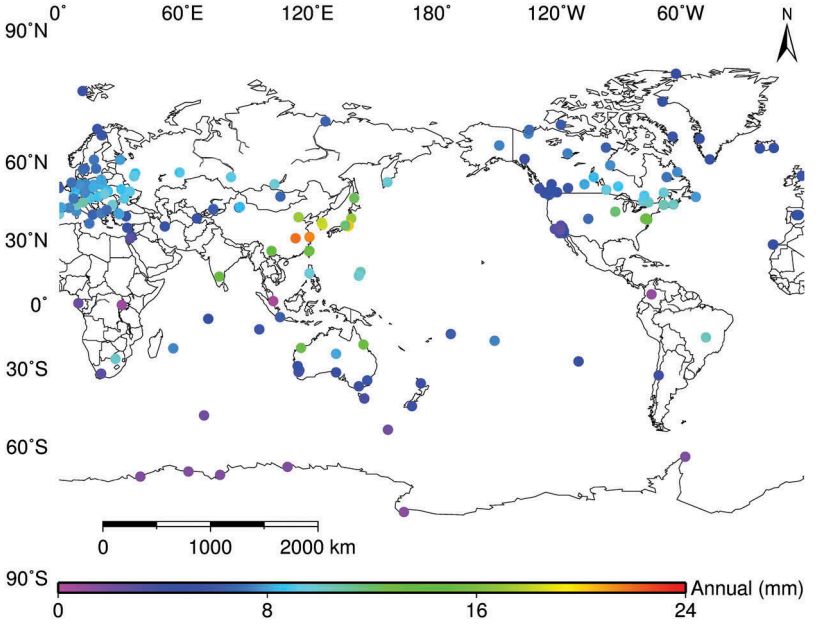

Figure 7. Geographical distribution of annual amplitude on a global scale.

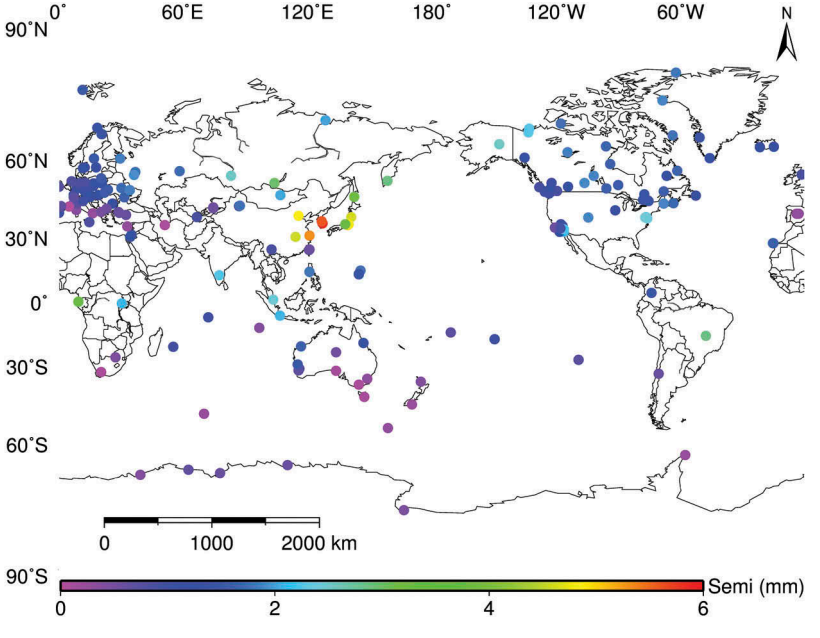

Figure 8. Geographical distribution of semi-annual amplitude on a global scale.

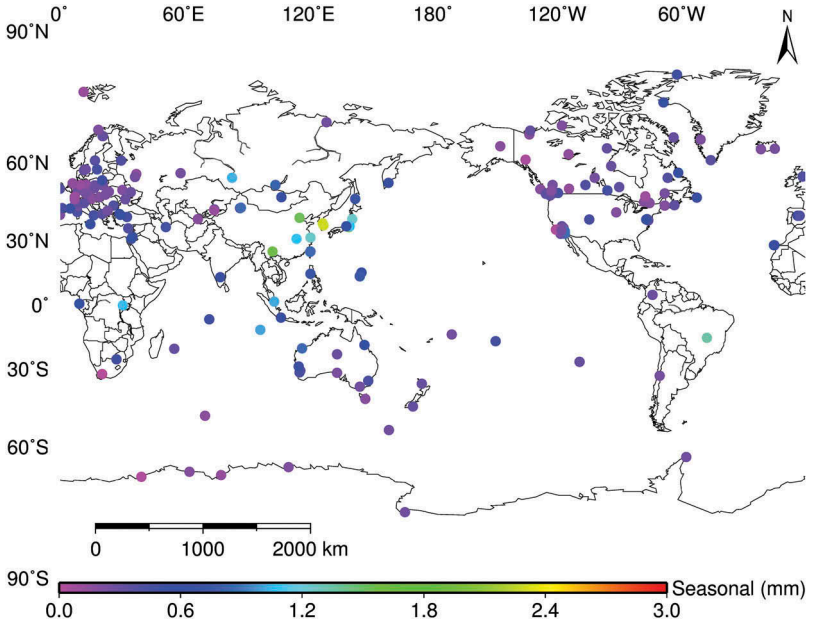

Figure 9. Geographical distribution of seasonal amplitude on a global scale.

different amplitudes in PWV time series data globally, which show the annual, semi-annual, and seasonal amplitudes range from 0 to 24 mm, 0 to 6 mm, and 0 to 3 mm, respectively. Due to the lower water vapour content, the annual, semi-annual, and seasonal amplitudes of PWV are very small in the South Frigid Zone with mean values of 1.8, 0.5, and 0.2 mm, respectively. In the South Temperate Zone, three types of amplitudes are relatively large with values of 4.4, 0.4, and 0.3 mm, respectively. In the Tropical and North Temperate zones, the amplitudes are similar with values of 7.2 mm and 8 mm, 1.7 mm and 1.5 mm, 0.7 mm and 0.4 mm, respectively, while the values decreased to 5.7, 1.7, and 0.3 mm, respectively, in the North Frigid Zone. Therefore, it can be concluded that the water vapour content is higher and the atmosphere more active in the Tropical and North Temperate zones, where anthropogenic activities are more frequent. The main component (annual or semi-annual oscillations) of the PWV periodic variations is also determined for the 192 stations, and the result shows that the almost all stations are mainly determined by the annual amplitude except for four IGS stations (NKLG, MBAR, NTUS, and BOGT), which are located near the equator (Figure 10). As mentioned in Section 3.2, those four sites have small RMS values, which is because the PWV variation is mainly determined by the semi-annual amplitude and the annual PWV variation is not large even though the water vapour content is very high at those four sites.

4.2. *Trend detection in PWV variations*

The trend in PWV variation for 192 stations is analysed based on the established PWV model in Section 2. Figure 11 shows the geographic distribution of PWV variation trends on a global scale. It can be observed that the trend in PWV variation was

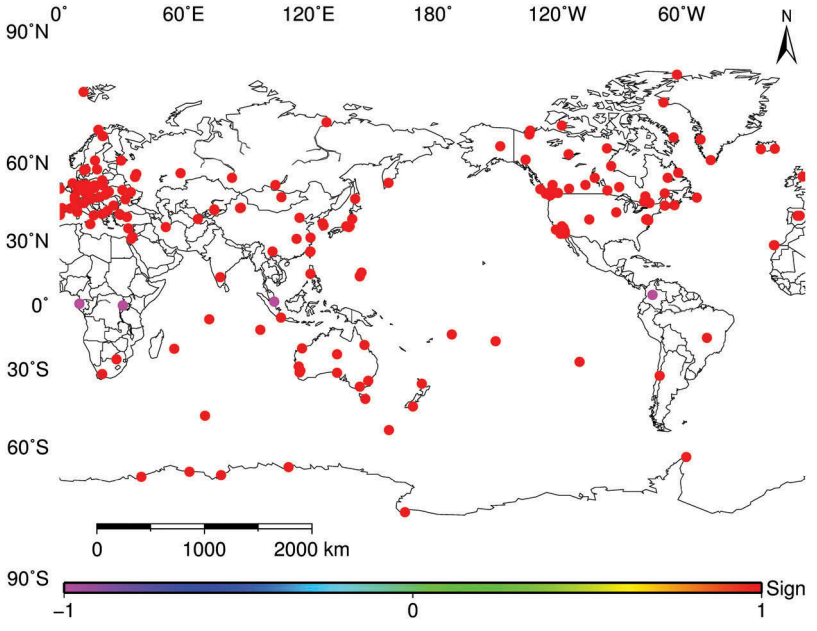

Figure 10. Geographical distribution of relationship between annual and semi-annual amplitudes on a global scale, where 'Sign = 1' means the annual amplitude is the main component while 'Sign = −1' means the semi-annual amplitude is the main component.

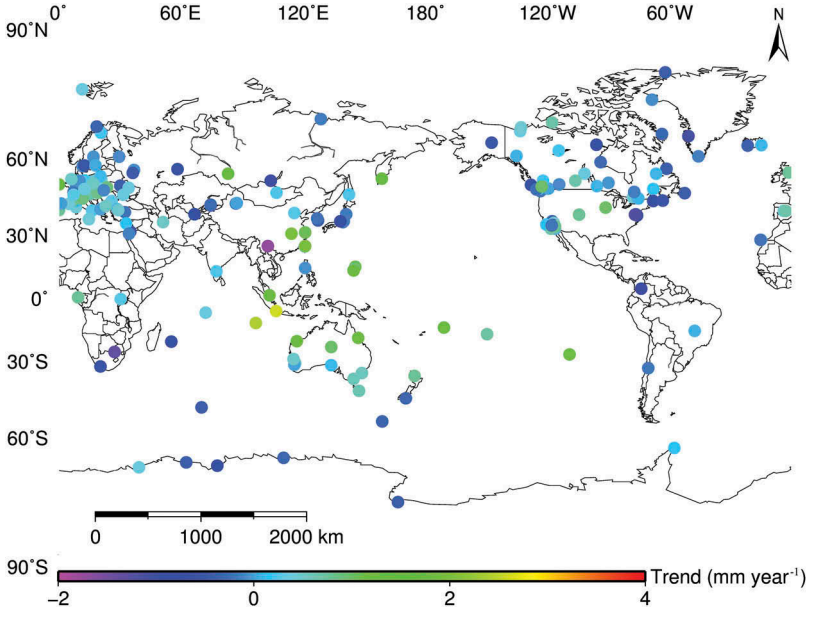

Figure 11. Geographical distribution of PWV variation trends on a global scale.

mostly negative in the South and North Frigid Zones while it was positive in the other three zones. In addition, the PWV variations in the Tropical Zone are greater than those in other zones. Statistical analysis reveals that PWV variations are

−0.27 mm year^{-} (Alshawaf et al. 2017) and −0.05 mm year^{-} (Alshawaf et al. 2017) in the South and North Frigid Zones and 0.18 $^{-}$ (Alshawaf et al. 2017), 0.17 $^{-}$ (Alshawaf et al. 2017), and 0.76 mm year^{-} (Alshawaf et al. 2017) in the North and South Temperate as well as Tropical Zones. It should be noted that the estimated trends may be inaccurate because these values depend on the length variations in the time series data (Alshawaf et al. 2017), and a period of 30 years is considered appropriate for averaging variations in such data (Arguez and Vose, 2011).

To further detect the trend in long-term PWV data, the Mann–Kendall method and Sen's slope estimation method are introduced. Here, the Mann–Kendall method, which is hardly affected by outliers and does not require distributional assumptions, is mainly used to perform significance testing using the calculated *Z*-values at the 95% significance level (Mann, 1945; Kendall, 1975). Sen's slope estimation method is used to judge the magnitude of upward or downward trends in the PWV time series (Sen, 1968; Tabari and Talaee, 2011). As shown in Figure 12, when the trend test was performed over the entire period (2004–2017), only 37 of 192 sites presented significant trends (confidence level: 95%) on a global scale. Sites in the North Frigid, North Temperate, and Tropical Zones show an increasing trend with the average values of 0.03 (Alshawaf et al. 2017), 0.13 (Alshawaf et al. 2017), and 0.14 mm year^{-} (Alshawaf et al. 2017), while the negative trend is observed in the South Temperate and South Frigid Zones with values of −0.04 (Alshawaf et al. 2017) and −0.02 mm year^{-} (Alshawaf et al. 2017), respectively. By analysing the distribution of Sen's slope on a global scale, we can conclude that the variation shows an upwards trend in continental regions, except for South America, southern Africa, and Antarctica.

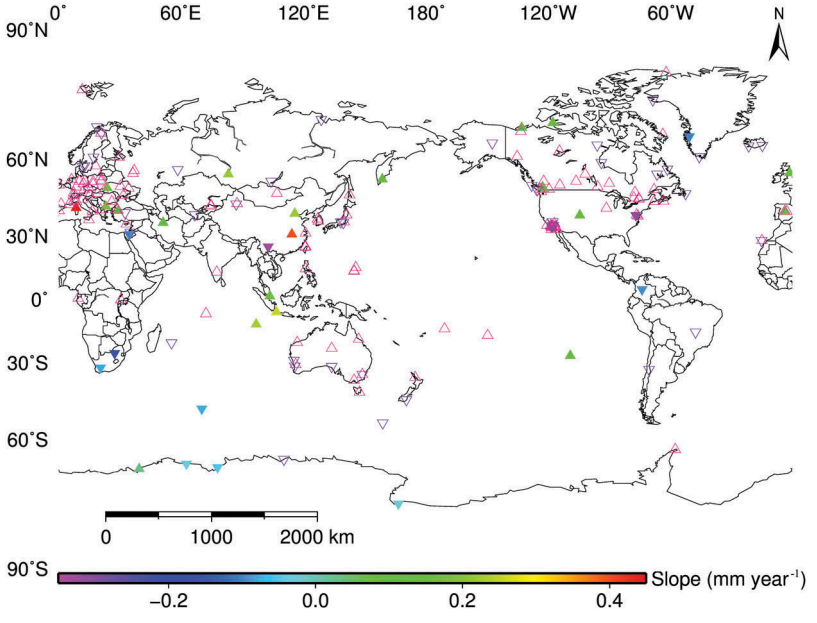

Figure 12. Map of the Mann–Kendal method and Sen's slope magnitude derived from the weekly PWV data from 2004 to 2017, sites with confidence level < 95% denoted by hollow triangles.

4.3. *Influence of anthropogenic activity on PWV variation*

Some studies have proved that anthropogenic activity affects the variation of several meteorological parameters, e.g. diurnal temperature range, relative humidity, the frequency of light rain, and PWV (Ho *et al*., 2009; Wong *et al*., 2015). The main effect is seen at weekends, which are considered as an indicator of anthropogenic activities. In this study, the weekend effects are defined as the average PWV value for Saturday through Monday minus the average PWV value from Monday to Friday. Because the anthropogenic activity is also affected by season, therefore, the weekend effects are analysed separately by season, where Spring lasts from March to May, Summer lasts from June to August, Autumn lasts from September to November, and Winter lasts from December to the February of the following year. A statistical analysis is performed for the PWV variation between weekday and weekend in four seasons to explore the relationship between the PWV variation and anthropogenic activity. The PWV variations of all stations globally are calculated and tested with the confidence level larger than 95%. In addition, the world population distribution is also considered to analyse the influence of anthropogenic activity on PWV variation, which is because the anthropogenic activity is affected by population density. By comparing the PWV differences at different stations in four seasons and the corresponding population density, the influence of human activities to PWV variations can be reflected to some extent.

Figure 13 shows the PWV differences between weekends and weekdays from 2004 to 2017 while values below 0.4 mm are deleted. The influence of anthropogenic activity on the PWV difference is differs by season, for example, weekend effects show a positive trend in the coastal area of south-eastern China in Spring and Autumn while the trend is reversed in Winter. Figure 14 shows that many people live in this area; therefore, this may be explained that anthropogenic activity is frequent in Spring and Autumn given better weather while activity is relatively infrequent with the temperature decreased in Winter. In the south-east of Canada and the north-east of the USA, both populous regions, weekend effects show the opposite effect in Spring and Summer while only positive effects can be found in western Europe in Winter. In addition, the number of sites with absolute PWV differences exceeding 0.4 mm is relatively large in the northern Hemisphere during Summer and this number decreased in Winter and vice versa in the Southern Hemisphere. Such behaviour is evidently affected by season, and the season further influences anthropogenic activity. Therefore, the PWV weekend effects act on a global scale and were found to be negative or positive, depending on season and region, which also suggested that complex mechanisms are factored in the PWV weekend effects.

5. Conclusion

In this study, a comprehensive analysis of long-term PWV data was performed on a global scale over the period from 2004 to 2017. The PWV time series was first calculated based on the IGS-derived ZTD and GGOS-derived surface pressure and atmospheric weighted temperature, and the RMS error of the calculated PWV values is about 1.28 mm globally. Periodic components of PWV time series data were detected based on the Lomb–Scargle periodogram method, and then a general PWV model is established considering the annual, semi-annual, and seasonal variations. The accuracy of the PWV model is also tested

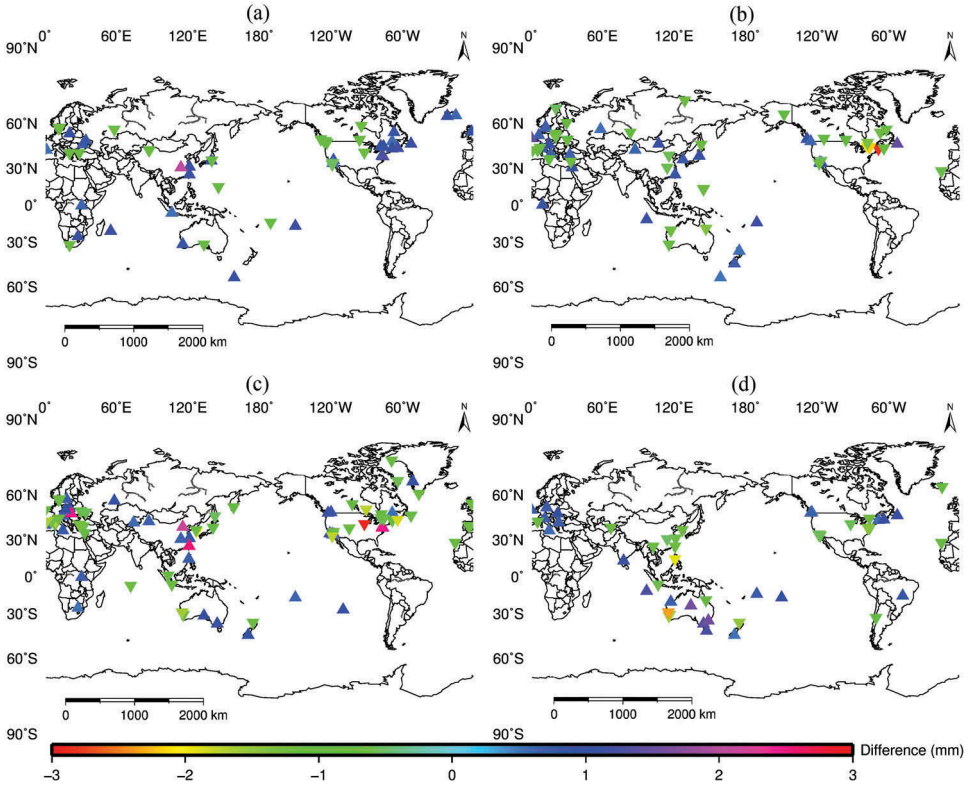

Figure 13. PWV difference between weekends and weekdays, where (a)–(d) represent Spring, Summer, Autumn, and Winter, respectively.

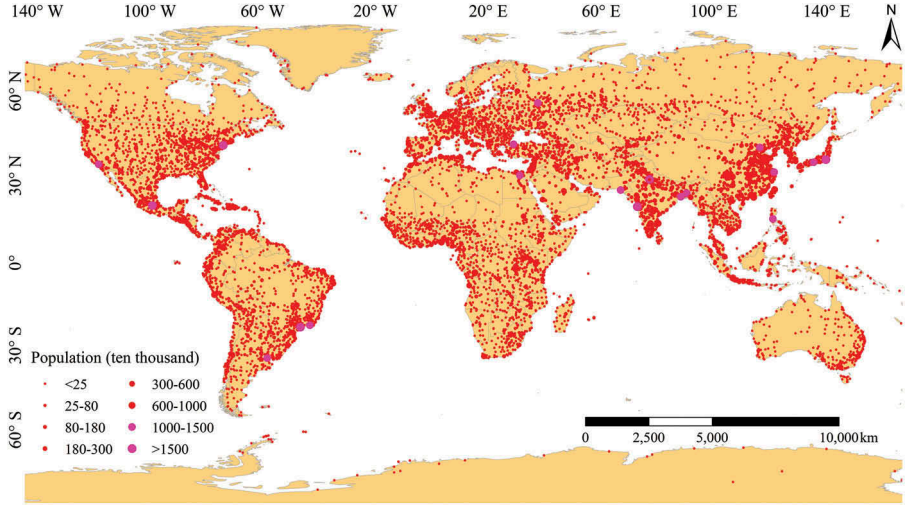

Figure 14. Map of world population distribution.

with the RMS error value of 4.10 mm. The characteristics of PWV mean values, annual, and semi-annual amplitudes were analysed on a global scale and the annual amplitude was found to have been the primary component driving PWV variations. The variations in PWV were also presented on the basis of the estimated trend component from the established PWV model as well as the Mann–Kendall trend test and Sen's slope estimator. Finally, the influence of anthropogenic activity on PWV variation was discussed and the influence of the weekend effects varied depending on different regions and seasons.

In conclusion, these findings are useful when trying to understand the characteristics of PWV spatio-temporal variations. In addition, the spatio-temporal analysis of PWV time series data on a global scale indicates the variation in climatic relationships and anthropogenic activities. This study provided some useful applications of PWV data in meteorology, climatology and other areas.

Acknowledgments

The authors would like to thank IGS for providing highly precise GPS ZTD products, the GGOS Atmosphere and IGRA are also thanked for providing the corresponding data. This research was supported by the Excellent Youth Science and Technology Fund Project of Xi'an University of Science and Technology (2018YQ3-12) and the Startup Foundation for Doctor of Xi'an University of Science and Technology (2017QDJ041).

Disclosure statement

No potential conflict of interest was reported by the authors.

Funding

This research was supported by the Excellent Youth Science and Technology Fund Project of Xi'an University of Science and Technology (2018YQ3-12) and the Startup Foundation for Doctor of Xi'an University of Science and Technology (2017QDJ041).

References

Alshawaf, F., K. Balidakis, G. Dick, S. Heise, and J. Wickert. 2017. "Estimating Trends in Atmospheric Water Vapor and Temperature Time Series over Germany." *Atmospheric Measurement Techniques* 10 (9): 3117–3132. doi:10.5194/amt-10-3117-2017.

Arguez, A., and R. S. Vose. 2011. "The Definition of the Standard WMO Climate Normal: The Key to Deriving Alternative Climate Normals." *Bulletin of the American Meteorological Society* 92 (6): 699–704. doi:10.1175/2010BAMS2955.1.

Askne, J., and H. Nordius. 1987. "Estimation Of Tropospheric Delay for Microwaves from Surface Weather Data." *Radio Science* 22 (3): 379–386.

Barman, P., S. Jade, A. Kumar, and W. Jamir. 2017. "Inter Annual, Spatial, Seasonal, and Diurnal Variability of Precipitable Water Vapour over Northeast India Using GPS Time Series." *International Journal of Remote Sensing* 38 (2): 391–411. doi:10.1080/01431161.2016.1266110.

Bevis, M., S. Businger, S. Chiswell, T. A. Herring, R. A. Anthes, C. Rocken, and R. H. Ware. 1994. "GPS Meteorology: Mapping Zenith Wet Delays Onto Precipitable Water." *Journal of Applied Meteorology* 33 (3): 379–386.

Bevis, M., S. Businger, T. A. Herring, C. Rocken, R. A. Anthes, and R. H. Ware. 1992. "GPS Meteorology: Remote Sensing of Atmospheric Water Vapor Using the Global Positioning System." *Journal of Geophysical Research: Atmospheres* 97 (D14): 15787–15801. doi:10.1029/92JD01517.

Böhm, J., A. Niell, P. Tregoning, and H. Schuh. 2006. "Global Mapping Function (GMF): A New Empirical Mapping Function Based on Numerical Weather Model Data." *Geophysical Research Letters* 33 (7).

Brettle, M. J., and J. F. P. Galvin. 2003. "Back to Basics: Radiosondes: Part 1 – the Instrument." *Weather* 58: 336–341.

Byun, S. H., and Y. E. Bar-Sever. 2009. "A New Type of Troposphere Zenith Path Delay Product of the International GNSS Service." *Journal of Geodesy* 83 (3–4): 1–7.

Ding, M., and W. Hu. 2017. "A Further Contribution to the Seasonal Variation of Weighted Mean Temperature." *Advances in Space Research* 60: 11. doi:10.1016/j.asr.2017.09.025.

Held, I. M., and B. J. Soden. 2000. "Water Vapor Feedback and Global Warming." *Annual Review of Energy and the Environment* 25 (1): 441–475. doi:10.1146/annurev.energy.25.1.441.

Ho, C. H., Y. S. Choi, and S. K. Hur. 2009. "Long-Term Changes in Summer Weekend Effect over Northeastern China and the Connection with Regional Warming." *Geophysical Research Letter* 36 (15): 15706. doi:10.1029/2009GL039509.

Hocke, K. 1998. "Phase Estimation with the Lomb-scargle Periodogram Method." *Annales Geophysicae* 16: 356–358.

Jade, S., and M. S. M. Vijayan. 2008. "GPS-based Atmospheric Precipitable Water Vapor Estimation Using Meteorological Parameters Interpolated from NCEP Global Reanalysis Data." *Journal of Geophysical Research: Atmospheres* 113 (D3). doi:10.1029/2007JD008758.

Jade S, Vijayan MSM, Gaur VK et al. 2005. "Estimates of Precipitable Water Vapor from GPS Data in Indian Subcontinent." *Journal Atmos Sol Terr Physical* 67 (6): 623–635. DOI:10.1016/j.jastp.2004.12.010.

Jakobson, E., H. Ohvril, and G. Elgered. 2009. "Diurnal Variability of Precipitable Water in the Baltic Region, Impact on Transmittance of the Direct Solar Radiation." *Boreal Environment Research* 14 (1): 45–55.

Jin, S., J. U. Park, J. H. Cho, and P. H. Park. 2007. "Seasonal Variability of GPS-derived Zenith Tropospheric Delay (1994–2006) and Climate Implications." *Journal of Geophysical Research: Atmospheres* 112 (D9). doi:10.1029/2006JD007772.

Joshi, S., K. Kumar, B. Pande, and M. C. Pant. 2013. "GPS-derived Precipitable Water Vapour and Its Comparison with Modis Data for Almora, Central Himalaya, India." *Meteorology & Atmospheric Physics* 120 (3–4): 177–187. doi:10.1007/s00703-013-0242-z.

Kendall, M. G. 1975. *Rank Correlation Methods*. Charles Griffin: London.

Kouba, J. 2015. "A Guide to Using International GNSS Service (IGS) Products." September 2015 update.

Liu, Z., M. S. Wong, J. Nichol, and P. W. Chan. 2013. "A Multi Sensor Study of Water Vapour from Radiosonde, MODIS and AERONET: A Case Study of Hong Kong." *International Journal of Climatology* 33 (1): 109–120. doi:10.1002/joc.v33.1.

Mann, H. B. 1945. "Nonparametric Tests against Trend. Econometrica." *Journal of the Econometric Society* 245–259. doi:10.2307/1907187.

Ortiz, De, Galisteo, J. P., V. Cachorro, C. Toledano, B. Torres, N. Laulainen, Y. Bennouna, and A. De, Frutos. 2011. "Diurnal Cycle of Precipitable Water Vapor over Spain." *Quarterly Journal of the Royal Meteorological Society* 137: 948–958. doi:10.1002/qj.v137.657.

Palau, J. L., F. Rovira, and M. J. Sales. 2017. "Satellite Observations of the Seasonal Evolution of Total Precipitable Water Vapour over the Mediterranean Sea." In *Advances in Meteorology*, 3–6.

Raval, A., and V. Ramanathan. 1989. "Observational Determination of the Greenhouse Effect." *Nature* 342 (6251): 758–761. doi:10.1038/342758a0.

Saastamoinen, J. 1972. "Atmospheric Correction for the Troposphere and Stratosphere in Radio Ranging Satellites." *The Use of Artificial Satellites for Geodesy* 15: 247–251.

Sen, P. K. 1968. "Estimates of the Regression Coefficient Based on Kendall's Tau." *Journal of The American Statistical Association* 63 (324): 1379–1389.

Tabari, H., and P. H. Talaee. 2011. "Recent Trends of Mean Maximum and Minimum Air Temperatures in the Western Half of Iran." *Meteorology and Atmospheric Physics* 111 (3–4): 121–131. doi:10.1007/s00703-011-0125-0.

Van Baelen, J., J. P. Aubagnac, and A. Dabas. 2005. "Comparison of Near–Real Time Estimates of Integrated Water Vapor Derived with GPS, Radiosondes, and Microwave Radiometer." *Journal of Atmospheric and Oceanic Technology* 22 (2): 201–210. doi:10.1175/JTECH-1697.1.

Wang, X., K. Zhang, S. Wu, S. Fan, and Y. Cheng. 2016. "Water Vapor-Weighted Mean Temperature and Its Impact on the Determination of Precipitable Water Vapor and Its Linear Trend." *Journal of Geophysical Research: Atmospheres* 121 (2): 833–852.

Wang, Z., X. Zhou, Y. Liu, D. Zhou, H. Zhang, and W. Sun. 2017. "Precipitable Water Vapor Characterization in the Coastal Regions of China Based on Ground-Based GPS." *Advances in Space Research* 60: 2368–2378. doi:10.1016/j.asr.2017.09.017.

Wong, M. S., X. Jin, Z. Liu, J. Nichol, and P. W. Chan. 2015. "Multi Sensors Study of Precipitable Water Vapour over Mainland China." *International Journal of Climatology* 35 (10): 3146–3159. doi:10.1002/joc.2015.35.issue-10.

Yeh, T. K., J. S. Hong, C. S. Wang, C. H. Chen, K. H. Chen, and C. T. Fong. 2016. "Determining the Precipitable Water Vapor with Ground-Based GPS and Comparing Its Yearly Variation to Rainfall over Taiwan." *Advances in Space Research* 57 (12): 2496–2507. doi:10.1016/j.asr.2016.04.002.

Yibin, Y., Z. Bao, X. Chaoqian and C. Jiajun. 2014. Analysis of The Global Tm-Ts Correlation and Establishment of the Latitude-Related Linear Model." *Chinese Science Bulletin* 59 (19): 2340-2347. doi:10.1007/s11434-014-0275-9.